A Comprehensive Computational Study of the Interaction between Human Serum Albumin and Fullerenes

ARTICLE *in* THE JOURNAL OF PHYSICAL CHEMISTRY B · NOVEMBER 2015

Impact Factor: 3.3 · DOI: 10.1021/acs.jpcb.5b05998

6 AUTHORS, INCLUDING:

Georgios Leonis

National Hellenic Research Foundation

22 PUBLICATIONS **90** CITATIONS

SEE PROFILE

Aggelos Avramopoulos

National Hellenic Research Foundation

54 PUBLICATIONS **569** CITATIONS

SEE PROFILE

Konstantinos D Papavasileiou

National Hellenic Research Foundation

11 PUBLICATIONS **34** CITATIONS

SEE PROFILE

Heribert Reis

National Hellenic Research Foundation

77 PUBLICATIONS **983** CITATIONS

SEE PROFILE

THE JOURNAL OF PHYSICAL CHEMISTRY B

Article

pubs.acs.org/JPCB

Comprehensive Computational Study of the Interaction between Human Serum Albumin and Fullerenes

Georgios Leonis,*[,†] Aggelos Avramopoulos,[†] Konstantinos D. Papavasileiou,[†] Heribert Reis,[†] Thomas Steinbrecher,[‡] and Manthos G. Papadopoulos*[,†]

[†]Institute of Biology, Pharmaceutical Chemistry and Biotechnology, National Hellenic Research Foundation, 48 Vas. Constantinou Ave., Athens 11635, Greece

[‡]Institut für Physikalische Chemie, KIT, Fritz-Haber Weg 2, 76131 Karlsruhe, Germany

Supporting Information

ABSTRACT: Human serum albumin (HSA) is the most abundant blood plasma protein, which transports fatty acids, hormones, and drugs. We consider nanoparticle−HSA interactions by investigating the binding of HSA with three fullerene analogs. Long MD simulations, quantum mechanical (fragment molecular orbital, energy decomposition analysis, atoms-in-molecules), and free energy methods elucidated the binding mechanism in these complexes. Such a systematic study is valuable due to the lack of comprehensive theoretical approaches to date. The main elements of the mechanism are binding to IIA site resulting in allosteric modulation of the IIIA and heme binding sites with an increase in α-helical structure of IIIA. Fullerenes displayed high binding affinities for HSA; therefore, HSA can be used as a fullerene carrier, facilitating any toxic function the fullerene may exert. Complex formation is driven by hydrogen bonding, van der Waals, nonpolar, charge transfer, and dispersion energy contributions. Proper functionalization of C_{60} has enhanced its binding to HSA by more than an order of magnitude. This feature may be important for biological applications (e.g., photodynamic therapy of cancer). Satisfactory agreement with relevant experimental and theoretical data has been obtained.

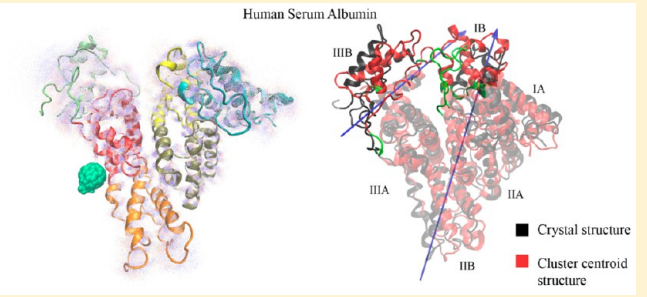

I. INTRODUCTION

Nanoparticle (NP) research comprises an ever growing field, owing to its broad range and specificity of technological and medicinal applications.[1] The latter have experienced significant achievements in recent years, with the development of various classes of drug delivery systems.[2] NPs' origin is either natural or engineered, crafted to possess well-defined shapes, sizes, physical, and chemical properties.[1] The broad array of NPs encompasses carbon (fullerenes, single- and multiwalled nanotubes), metal (gold colloids, nanoshells, nanorods, and superparamagnetic iron oxide NPs), and semiconductor-based (quantum dots) materials.[3] Their small size, which ranges from 1 to 100 nm in two or three dimensions,[3] allows for penetration in almost all levels of living organisms,[4] namely, cells, tissues, and organ systems. Upon entry, NP absorption occurs through interaction with biological fluids, such as blood plasma,[5] which contains diverse biomolecules.[6] NPs' compatibility with blood plasma proteins is essential for achieving in vivo functionality; otherwise, unwanted effects, such as coagulation and clot formations, are triggered.[5] Furthermore, NP toxicity drastically affects their biomedical potential[3] and is altered by the above factors, that is, physicochemical characteristics and protein absorption; a fundamental understanding of NP interactions with plasma proteins is therefore critical.[5]

Carbon-based NPs and especially fullerenes have attracted attention, mostly due to their unique physicochemical features,[7,8] which allow for engineering of functionalized derivatives, capable of "grafting nucleic acids, peptides and even proteins".[7] It is currently known that more than 20 proteins form stable complexes with fullerenes, both pristine and functionalized.[9−11] Pristine fullerenes are characterized by their inherent insolubility;[12] to this end, water-soluble fullerene-based derivatives have been widely investigated.[13] Fullerenes display a wide variety of shapes and sizes, exhibiting great potential in numerous biological and medicinal applications,[12,14,15] especially as drug delivery vectors[7] in targeted disease treatment[14,16,17] as well as antibacterial, antiviral, and neuroprotective agents.[13]

Human serum albumin (HSA) is an abundant protein in blood plasma,[6] while it is also present in various human body organs, such as skin, muscle, gut, and liver.[18] HSA lies in the epicenter of research that aims at pharmacokinetic profile improvement of targeted drug delivery,[19,20] given its integral role in ligand transport and distribution.[21] Such ligands include fatty acids, amino acids, hormones, drugs, as well as NPs.[22]

Received: June 23, 2015
Revised: October 2, 2015

DOI: 10.1021/acs.jpcb.5b05998
J. Phys. Chem. B XXXX, XXX, XXX−XXX

HSA comprises 585 residues, which are arranged to form a heart-shaped molecule, divided in three domains (Figure 1a).[23]

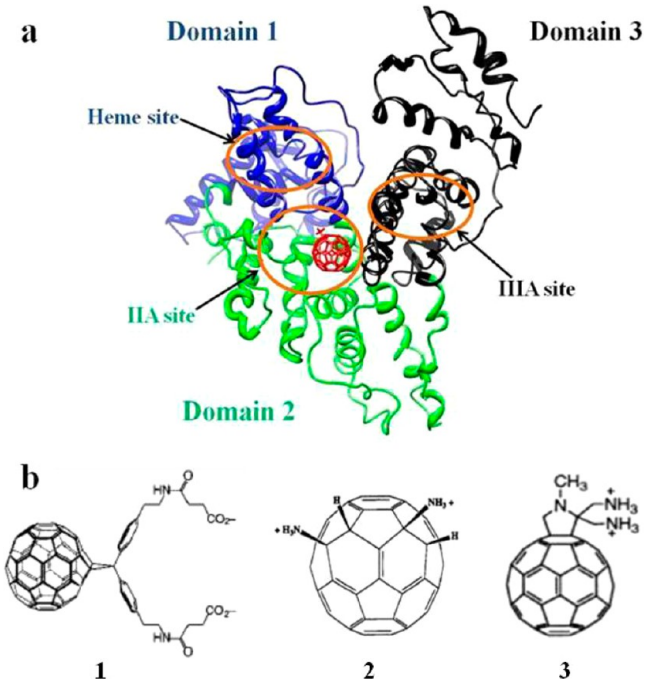

Figure 1. (a) Fullerene derivative **2** into the binding cavity IIA of the HSA crystal structure.[23] The three domains of the protein are shown in different colors. Binding site IIA belongs to domain 2, while IIIA and the heme binding sites are located at domains 3 and 1, respectively. (b) Chemical structures of fullerene derivatives **1**–**3** studied in this work.

Three HSA binding sites have been identified, namely, IIA (region including Trp214, His288, His440, Figure 1a), IIIA (Glu383, Arg410, Tyr411, Leu430, Val433), and the heme binding site (Arg114, Tyr138, Ile142, His146, Tyr161, Arg186).[24]

Numerous HSA complexes with fullerenes have been previously reported in the literature, involving experimental[22,25−31] and molecular dynamics (MD) studies.[30] For example, the HSA complex with a tris-malonic acid fullerene isomer[32] was found to be particularly stable, with a binding constant comparable to organic molecules, which strongly bind to the same site,[32,33] namely, the pocket formed in subdomain IIA of HSA.[34] Furthermore, HSA interacts with a water-soluble fullerene bearing phosphate residues[22] as well as a carboxy-C_{60}-fullerene.[25] Also, fullerene derivatives have been tested as carriers for serum protein profiling.[15,35]

The underlying theme of these studies can be summarized into two points: (a) fullerene−HSA complex formation is favorable and (b) fullerene's binding to HSA leads to conformational changes,[28,33] especially with regard to its secondary structure content,[25] without loss of its native structure.[25,30] For instance, in the cases of pristine fullerene and fullerol, the α-helical content of HSA was found to decrease,[26,28,30] whereas in the case of the organophosphate fullerene, the α-helical content of HSA increased.[22] Therefore, the effect of fullerene derivatives' functionalization on HSA structure remains an open question. Conservation of HSA's native structure upon fullerene binding is of paramount importance for maintaining both its functionality and its ability to transverse through the blood serum to reach tissues and organs, which are not directly accessible.[30] Furthermore, fullerene interactions with biological systems remain contradictory as several reports emphasize their potential harmfulness,[36] while in vivo studies indicate that fullerene and its derivatives exhibit low toxicity.[37] Hence, these concerns call for a detailed understanding of the mechanisms governing fullerene interactions with proteins and HSA in particular. Understanding such interactions may allow their modification in a way that the activity of the chosen fullerene analog is optimized.

It is known that fullerenes are very efficient $^1O_2$−generators. Singlet oxygen can damage DNA. It has been reported that, "The generation of singlet oxygen close to DNA can lead to oxidation of guanine residues, and the unpaired lesions can constitute pre-mutational events leading mainly to G → T transversions."[38] Thus, binding of C_{60} derivatives to HSA, which is a very efficient carrier, may facilitate their bioactivity (in the presence of light) against DNA. In this context, the phototoxicity of fullerenes has been used for therapeutic purposes; for example, carboxy-C_{60} bound to HSA has been employed as a photosensitizer for photodynamic cancer therapy.[39,40]

For this study, we have selected from the literature three fullerene analogs (shown in Figure 1b) according to the following criteria (references are provided in the Supporting Information):

(1) They have been implicated in interacting with biomolecular systems.
(2) They have been synthesized and display significant solubility in water.
(3) They possess side chains that may favor interactions with proteins.
(4) They represent different charge states.

This work aims at the discovery of the main elements of HSA binding mechanism with the above fullerene derivatives, and this mechanism will be used to rationalize the significant binding observed for some fullerene−HSA complexes. Structural and energetic data will be considered by employing a large array of computational techniques based on molecular dynamics (MD) and quantum mechanical (QM) methods. The combination of techniques allows us to approach the variations of fullerene−HSA upon binding at different levels of approximation and thus to illuminate various aspects of the complex. To date, extensive computational studies regarding fullerene−HSA systems have not been reported. Consequently, such a comprehensive approach is of particular importance toward the elucidation of nanoparticle−HSA interactions.

II. METHODS

The study of fullerene−HSA complexes has been attempted by applying an integrated computational approach, which combines classical methodologies (docking, MD, MM−PBSA) with rigorous QM techniques (fragment molecular orbital, energy decomposition analysis, and atoms-in-molecules). This work involves an extensive computational experimentation; however, because of space limitations, a considerable part of the data has been transferred to the Supporting Information.

II.1. Molecular Docking Calculations. Docking compounds **1**–**3** and pristine C_{60} into HSA was performed with the DOCK 6.4 program.[41,42] Compounds were considered flexible

DOI: 10.1021/acs.jpcb.5b05998
J. Phys. Chem. B XXXX, XXX, XXX−XXX

during docking and the DockPrep module was used for the albumin preparation.

II.2. Molecular Dynamics Simulations in Water. The complexes of HSA with the three fullerene analogs (Figure 1b) and C_{60} (each bound to IIA and IIIA sites) were subjected to unrestrained MD simulations in explicit water, with the AMBER 12 suite.[43,44] The 2.8 Å resolution crystal structure of the protein was obtained from the Protein Data Bank (ID: 1UOR).[23] Crystal water molecules were kept for the simulations and missing hydrogen atoms were added with AMBER. The General Amber Force Field (GAFF)[45] and ff99SB[46] were used to represent fullerenes and HSA, respectively, while the RESP procedure has been followed to assign atomic partial charges to fullerenes. The complexes were neutralized and then solvated with the TIP3P water model[47] in a truncated octahedral box (at least 10 Å distance between any atom of the complex and the box boundaries). After minimization, each system was heated in constant volume, until the target temperature of 310 K was reached. The MD simulations were performed under NPT conditions using a Langevin dynamics temperature scheme.[48] The GPU (CUDA) version of PMEMD in AMBER 12 was used to produce ∼10 ns/day on NVIDIA graphics cards.[49−51] All bonds involving hydrogen atoms were constrained[52] to their equilibrium distance. Initially, 100 ns MD simulations were performed for each HSA complex (**1**−**3**, C_{60}) and for the apo form of the protein; however, the unconverged simulations for complexes **1**−**3** during this time necessitated the prolongation (up to 500 or 550 ns) of the calculations to achieve better sampling of the conformational space. The resulting trajectories were analyzed in terms of their Cα RMSD and RMS fluctuations as well as radii of gyration and HB patterns. Moreover, **1**−**3** complexes as well as the apo HSA were processed by clustering, secondary structure, and dynamic domain motion analyses. Clustering was performed by imposing a 2.5 Å RMSD cutoff, using the *gromos* algorithm[53] as implemented within the *g_cluster* utility of the GROMACS 4.6.4 software.[54] Cluster centroid conformers were compared against the HSA crystal structure to examine qualitatively whether binding induces domain motions, by means of the DynDom server.[55] Further details of the analyses are presented in the Supporting Information.

II.3. MM−PBSA Calculations. This method calculates the interaction energy in the gas phase with molecular mechanics and estimates the solvation free energy by solving the Poisson−Boltzmann equation.[56,57] Normal mode analysis is used for the evaluation of the conformational entropy. The equations of the MM−PBSA scheme can be found elsewhere.[58]

Molecular mechanics Poisson−Boltzmann surface area (MM−PBSA) and molecular mechanics generalized Born surface area (MM−GBSA) methodologies have been widely used over the years to calculate binding free energies in various protein−ligand systems. Although absolute binding energy calculations with MM−PB(GB)SA often fail to reproduce the experimental results, it has been shown that the method performs well in predicting relative binding energies.[59] The practical use of MM−PB(GB)SA in lead discovery has been demonstrated by proposing new potential inhibitors of p38 MAP kinase and of HIV-1 RT.[60] Also, MM−PBSA was particularly successful in predicting the activity of new sirtuin inhibitors,[61] SUMO activating enzyme 1 inhibitors,[62] acetylcholinesterase inhibitor,[63] and an HIV-1 gp 41 fusion peptide inhibitor.[64] In a recent study, 28 crystal structures involving aldose reductase inhibitors were used to test the accuracy of the method.[65] It was shown that experimental and calculated binding free energies were correlated despite the fact that prediction of absolute free energies was unattainable.

The combination of MD and MM−PBSA approaches as described here has been applied by our group to several protein systems, including HIV-1 PR, renin, and κ-opioid receptor complexes, and the reliability of this procedure has been verified (average error between experimental and predicted binding energy values being <7%).[66]

II.4. Fragment Molecular Orbital Method. The fragment molecular orbital (FMO) approach allows performing ab initio calculations on quite large systems, using a limited number of approximations. The method is similar to the energy decomposition analysis (EDA) pioneered by Morokuma[67,68] and is described in ref 69. Here the FMO analysis was performed for two **2**−HSA complexes (**2** bound to IIA or IIIA) in vacuum and aqueous medium. A full decomposition of the interaction energy (eq S1) was performed with the Pair Interaction Energy Decomposition Analysis (PIEDA),[70] as implemented in GAMESS.[71] Details of the application of the FMO method to the fullerene complexes are provided in the Supporting Information.

II.5. Energy Decomposition Analysis. Two schemes have been employed for the resolution of the interaction energy. These methods provide an insight into the effect of the terms (e.g., electrostatic, polarization, dispersion) involved in the interaction mechanism.

The first approach is based on the method developed by Su and Li.[72] According to this, the interaction energy (ΔE) is given by the following equation

$$\Delta E = E_{el} + E_{ex} + E_{rep} + E_{pl} + E_{disp} \quad (1)$$

where E_{el} is the electrostatic term (classical Coulomb interaction between monomers), E_{ex} is the exchange contribution (exchange terms between monomers), and E_{rep} is the repulsion term. The polarization term, E_{pl}, describes the "orbital relaxation energy" going from the monomer HF spin orbitals to those of the supermolecule. The dispersion energy term, E_{disp}, is the difference between the MP2 and HF interaction energies.

The second approach is based on the decomposition scheme developed by Kitaura and Morokuma (KM),[67] where the interaction energy ΔE can be written as follows

$$\Delta E = E_{el} + E_{xr} + E_{ct} + E_{pl} \quad (2)$$

E_{el}, E_{xr}, E_{ct}, and E_{pl} correspond to the classical electrostatic, exchange-repulsion, charge transfer, and polarization contribution, respectively.[67] At the HF level, the E_{el} terms of eqs 1 and 2 are identical, the sum of E_{ex} and E_{rep} (eq 1) equals the exchange-repulsion in KM, while the E_{pl} term (eq 1) equals the sum of polarization, charge transfer, and a mixing term (contribution to the interaction energy including the coupling interaction between components) of the KM analysis.[67]

Both energy decomposition analysis (EDA) schemes were carried out in the gas phase by employing the GAMESS code. The correction due to the basis set effect has also been considered using the counterpoise method of Bernardi and Boys.[73]

II.6. Atoms-In-Molecules Method. The Atoms In Molecules (AIM)[74] approach has been used to compute the energy of hydrogen bonds (HBs).[75] It is based on changes in the electron distribution, resulting by either bond or complex formation, thus providing insight into the nature of the

DOI: 10.1021/acs.jpcb.5b05998
J. Phys. Chem. B XXXX, XXX, XXX−XXX

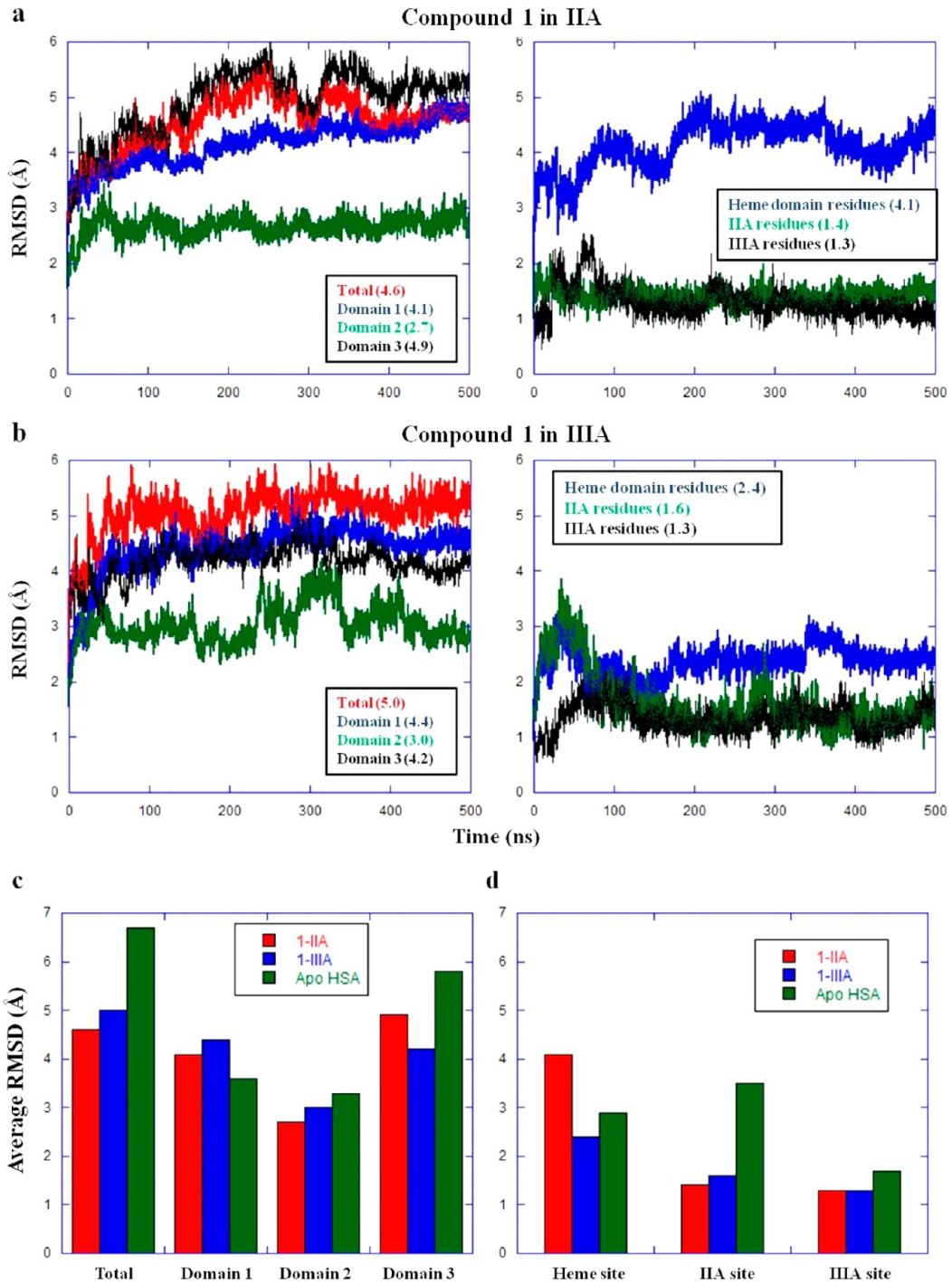

Figure 2. RMSD for Cα atoms of HSA residues with fullerene derivative **1** bound to (a) IIA and (b) IIIA binding sites. RMSD plots are shown with respect to different HSA regions: the entire protein, domain 1 (residues 20−195, Figure 1a), domain 2 (residues 196−383, Figure 1a), domain 3 (residues 384−575, Figure 1a), and IIA, IIIA, and heme sites. Average RMSD values (in parentheses) are shown in panels c and d.

chemical bond. The electron density distribution function was computed with GAUSSIAN 09 at the MP2/6-31G* level of theory,[76] while all bond critical points, Laplacians, and the kinetic energy were computed with AIM2000.[77] Details of the method are provided in refs 78 and 79.

III. RESULTS AND DISCUSSION

In this section, we present the conformational, HB, and energetic results, as obtained from the MD and MM−PBSA calculations on the fullerene−HSA complexes (Figure 1) and pristine C_{60} (each bound to IIA and IIIA sites); **2** was also included in the heme site. Indicatively, to account for higher (more rigorous) levels of approximation, these results were complemented by QM (FMO, EDA, and AIM) calculations on **2**−HSA complex. We have obtained a collection of MD trajectories that correspond to multiple-length (100, 200, 500, and 550 ns) simulations for the **1**, **2**, **3**, and C_{60} HSA systems (total simulation time 3.3 μs).

III.1. Structural Analysis of HSA Complexes. This part includes the investigation of the structural variation in HSA

DOI: 10.1021/acs.jpcb.5b05998
J. Phys. Chem. B XXXX, XXX, XXX−XXX

Table 1. Average RMSD Values (Å) for Selected HSA Regions of Complexes with 1−3 and C_{60}

complex		total	Domain1	Domain2	Domain3	heme site	IIA site	IIIA site
1	IIA[a]	4.6	4.1	2.7	4.9	4.1	1.4	1.3
	IIIA[b]	5.0	4.4	3.0	4.2	2.4	1.6	1.3
2	IIA	5.4	4.7	3.3	5.0	3.4	2.5	1.5
	IIIA	4.5	4.0	3.1	3.9	3.0	1.7	1.4
	heme site	5.4	4.4	3.0	4.0	3.6	2.8	1.3
3	IIA	6.0	4.8	2.7	5.6	3.2	1.4	1.4
	IIIA	6.1	3.8	3.6	5.5	1.6	2.6	1.6
C_{60}	IIA	5.6	4.2	2.7	5.6	1.8	1.6	1.8
	IIIA	3.9	3.4	2.3	3.6	2.4	1.6	0.9
Apo HSA		6.7	3.6	3.3	5.8	2.9	3.5	1.7

[a]Fullerene analog **1** bound to the IIA site of HSA. [b]Fullerene analog **1** bound to the IIIA site of HSA.

complexes with **1**−**3** and C_{60} by means of RMSD, radius of gyration, clustering, fluctuations, secondary structure, and dynamic domain analyses.

RMSD Calculations. Conformational analysis on the trajectories of albumin complexes with compounds **1**−**3** has been performed for the Cα atoms of specific HSA regions. The results are presented in Figures 2−5 (parts a−d) and Table 1, which summarizes the average RMSD values for HSA regions in its apo and fullerene-bound forms. As anticipated, apo HSA is more variable and slightly more "expanded" than its bound forms (Table 1 and Table S1, Figures 2−5 and Figure S1). The increased changeability of apo HSA is denoted by the higher average total RMSD value (6.7 Å) compared with the protein structures in complexes with **1**−**3** (Table 1). A proper measure of the average size of a protein is the radius of gyration, which provides a quantitative estimation on the relative compactness of a structure. As shown in Table S1, the radii of gyration for all fullerene−HSA complexes are lower than the radius of gyration of the apo protein. Regarding the structures of the ligands, it was observed that **1**−**3** are very confined into either binding site. The two active site regions of HSA (IIA and IIIA) also appear particularly stable either in the apo or in the complexed form (RMSD < 0.8 Å in all cases). To account for the effect of polar groups on the fullerene−HSA interactions, we have also studied the binding of the fullerene core (C_{60}) to the two sites of albumin. It was shown that C_{60} is incorporated in IIA or IIIA in a way that HSA is stabilized (Figure S2a,b). Indeed, the average RMSD values for the two C_{60}−HSA complexes are lower than the corresponding values of the apo form and resemble the calculations for complexes **1**−**3** (Table 1). The only exception involves domain 1 (upon C_{60} binding to IIA), which is slightly more mobile than in the apo form. Additionally, a conformational change that may have destabilized the complex was observed after ∼50 ns on the heme domain, when C_{60} was bound to IIIA (Figure S2b). The three binding sites appear very stable, which resulted in a less expanded structure for HSA compared with the apo form (Table S1). Also, the fullerene core into either IIA or IIIA was practically stable, with RMSD values being lower than 0.1 Å, which indicated efficient HSA binding for C_{60}.

Clustering. Clustering analysis on complexes with **1**−**3** as well as the apo HSA revealed that binding to IIA subdomain leads to a smaller number of clusters (NOC) compared with the apo form (Table S2). Clustering results provide an alternative perspective of the RMSD analysis, showing that upon binding the HSA structure becomes less changeable. This agrees with the experimental work of Zhang et al., where IIA binding of an organophosphate-containing C_{60} derivative led to a more rigid and compact HSA structure.[22] On the contrary, NOC of **1** and **2** bound to IIIA are comparable to their apo form counterparts (Table S2), while **3** yielded low NOCs when bound to either IIA or IIIA. More information on the clustering analysis is provided in the Supporting Information.

Secondary Structure analysis. HSA secondary structure analysis (Figure S4a) indicated that **1**, **2**, and **3** binding to either IIA or IIIA does not alter the overall protein's secondary structure significantly compared with the apo form, which was also observed experimentally for pristine fullerene.[30] Nevertheless, a close inspection of particular regions reveals that they undergo subtle secondary structure changes upon fullerene binding (Figure S4b−d). For example, binding of **1**, **2**, and **3** to IIA leads to an increase in helical content in the vicinity of IIIA by 12.0, 25.4, and 28.7%, respectively (Figure S4c); this is indicative of allosteric modulation. Detailed discussion on the secondary structure analysis is provided in the Supporting Information.

HSA Flexibility. Regarding the mobility of individual HSA regions, the IIA sites and most of IIIA sites are more stable in the complexes than in the apo form (Figure 5a−c). The IIIA-bound form induces greater changes to the total structure of the protein compared with the IIA-bound form, except in the case of **2**; the (IIA site-containing) domain 2 is the most stable region among the three HSA domains in either complex, while the (IIIA site-containing) domain 3 appears to be significantly altered in most complexes; however, domain 3 in apo HSA is also the most unstable part of the protein (avg. RMSD = 5.8 Å) compared with domains 1 (avg. RMSD = 3.6 Å) and 2 (avg. RMSD = 3.3 Å). Importantly, we note that in HSA complexes with **2** and **3**, the IIA-bound form induces conformational changes to domain 1 (Figures 3 and 4) and for the complex with **2** specifically to the heme binding site residues at ∼270 ns of the simulation. This was not observed in the IIIA-bound form or even in the apo HSA (Figure S1). Therefore, IIA-binding in HSA is directly implicated in allosteric modulation of the heme binding site. The above findings are in agreement with other studies: it has been suggested that binding of several coadministered drugs to IIA site, such as anti-Parkinson's disease apomorphine and benserazide, is allosterically linked to the heme site.[80] Guizado performed clustering on 42 drug−HSA complexes to reveal that two major conformations exist regardless of the nature of the ligand or the position of the binding site;[81] domain 2 was particularly rigid, while the difference between the two structures can be described through "twist" and "hinge" relative motions of domains 1 and 3, respectively. Additional support was provided by other investigations, where crystal structures complexed with fatty

DOI: 10.1021/acs.jpcb.5b05998
J. Phys. Chem. B XXXX, XXX, XXX−XXX

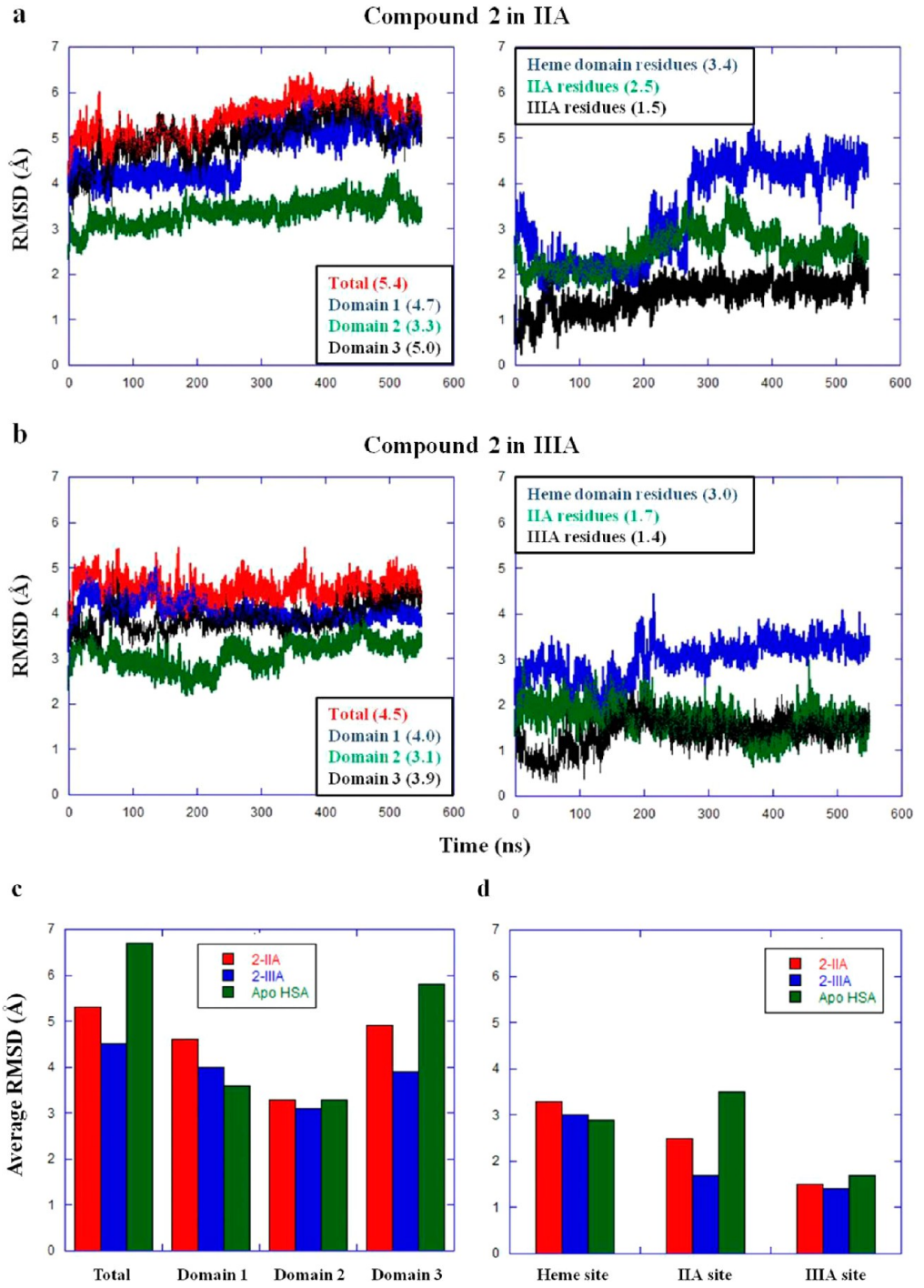

Figure 3. RMSD for Cα atoms of HSA residues with fullerene derivative **2** bound to (a) IIA and (b) IIIA binding sites. RMSD plots are shown with respect to different HSA regions: the entire protein, domain 1, domain 2, domain 3, and IIA, IIIA, and heme binding sites. Average RMSD values (in parentheses) are represented graphically in panels c and d.

acids also showed that domains 1 and 3 rotate with respect to domain 2.[82−85]

Dynamic Domain Analysis. To gain a better perspective of the conformational changes induced upon **1**−**3** binding to IIA and IIIA subdomains, the DynDom server was used,[55] without prior specification of fixed and moving domains. Dynamic domain analysis (DDA) ascribes rigid-body movement as a screw motion, comprising rotation and translation about and along an axis, respectively.[55] DDA involved the centroid structure of the longest living cluster of all simulations, namely, Cluster ID:1 as Conformer 2, against the crystal structure of HSA (Conformer 1). Even though this is a rather simplistic approach, it provided helpful insight into revealing HSA dynamics of both bound and unbound forms. DDA showed that the IIIB subdomain of the apo HSA centroid is displaced compared with its crystal structure. This rather complex conformational change is primarily characterized by an outward pivotal rotation of IIIB, leading to a less compact conformation (Figure S5a,b). This dislocation of the IIIB subdomain agrees with recent theoretical studies on HSA[86,87] and also appears to

DOI: 10.1021/acs.jpcb.5b05998
J. Phys. Chem. B XXXX, XXX, XXX−XXX

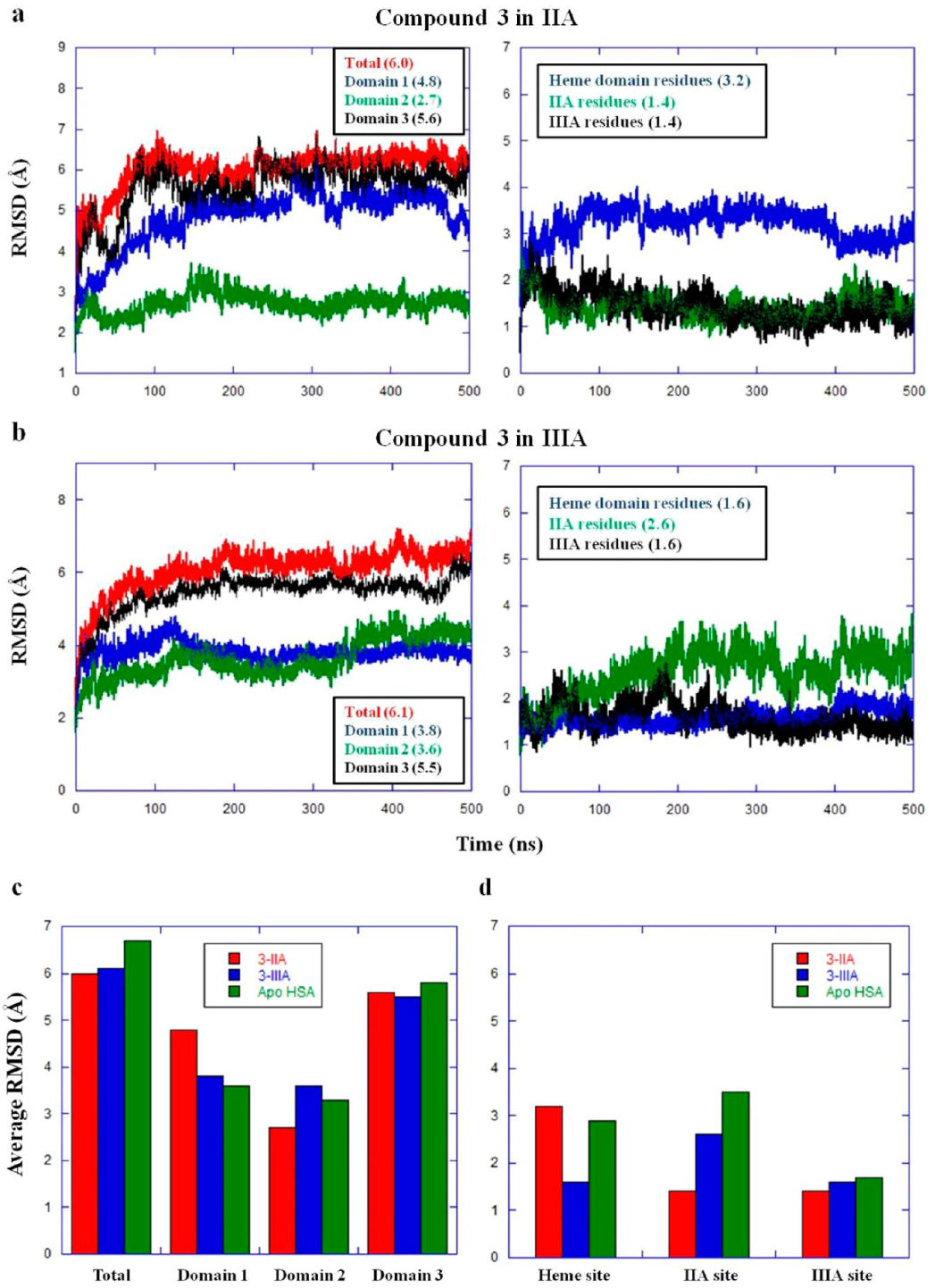

Figure 4. RMSD for Cα atoms of HSA residues with fullerene derivative **3** bound to (a) IIA and (b) IIIA binding sites. RMSD plots are shown with respect to different HSA regions: the entire protein, domain 1, domain 2, domain 3, and IIA, IIIA, and heme sites. Average RMSD values (in parentheses) are shown in panels c and d.

be a shared feature among the HSA−fullerene complexes analyzed. It was found that binding of **1** (Figure S6), **2** (Figure 6), **3** to IIA (Figure S7), and **3** to IIIA (Figure S8) results in a profound inward motion of the IIIB subdomain, characterized by a rotation in the range of 45.5−68.9° and an average interdomain closure by 83.1% for all three compounds. The main difference compared with the apo form is that the HSA structure becomes more compact; this domain movement has also been identified as a result of several ligands' binding to IIA.[81] Binding of **2** and **3** to IIA is characterized not only by this IIIB motion but also by the complementary movement of the IB and IA subdomains by an inward 53.0° and outward 80.5° rotation, respectively, with respect to the fixed domain (Figure 6 and Figure S7). In particular, the movement of residues 125−169 in the IIA-bound **2** complex and residues 74−103 in the IIA-bound **3** complex is depicted in Figure 5b,c (green), respectively. In addition to the aforementioned studies,[81−85] this correlated I−III domain motion resembles the structural

DOI: 10.1021/acs.jpcb.5b05998
J. Phys. Chem. B XXXX, XXX, XXX−XXX

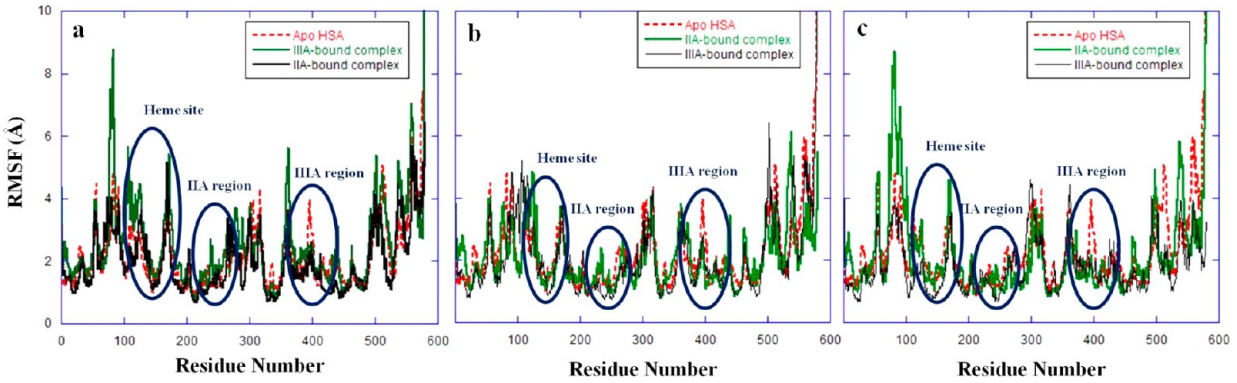

Figure 5. Cα atomic fluctuations of HSA residues in IIA-bound, IIIA-bound, and apo forms in complexes with (a) Compound **1**, (b) Compound **2**, and (c) Compound **3**.

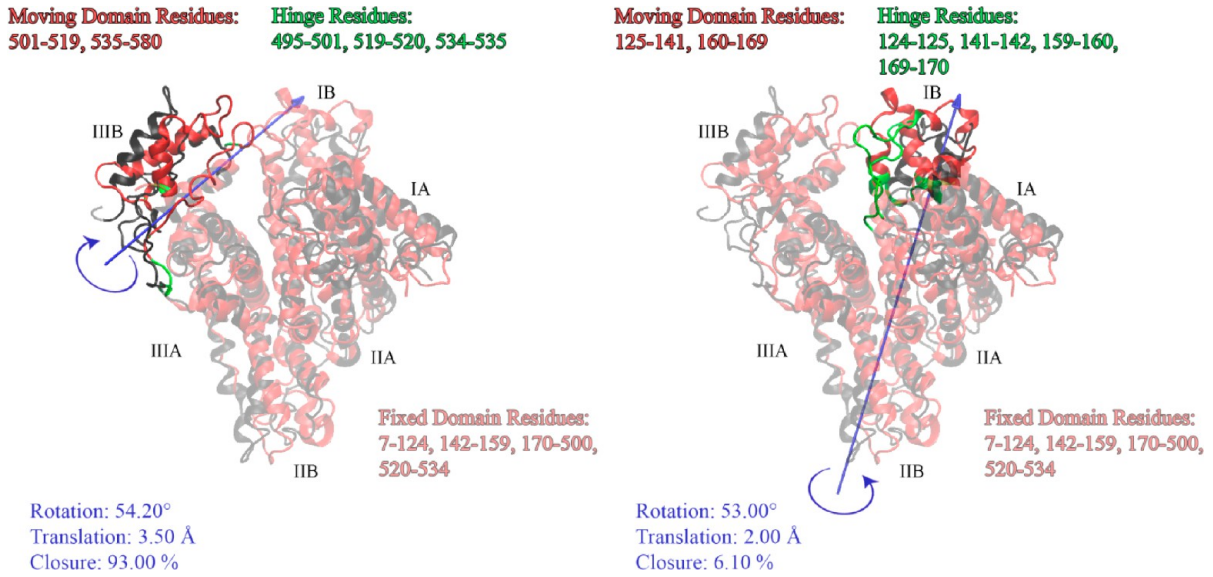

Figure 6. Results of the dynamic domain analysis performed on HSA having compound **2** bound to the IIA site. Screw axis is depicted by a blue arrow. Bending residues are colored green. The rigid protein domain is transparent, while the moving subdomains IIIB and IB are illustrated opaque. The IIA-bound form (red) is compared with the reference HSA crystal structure (black). A movie file illustrating domain movements is available in the Supporting Information.

behavior of the HSA–myristate complex, as predicted by Fujiwara et al.[86] No dynamic domains were identified for **1** and **2** at IIIA, and thus the HSA structure remains close to its native conformation. Details of the DDA are shown in the Supporting Information.

III.2. Hydrogen Bonding Interactions. The hydrogen bond analysis on the HSA complexes with **1**–**3** revealed that the fullerenes are stabilized in the binding sites through multiple and diverse HBs. Compound **1** forms several different HBs with binding cavity residues (Figure 7a), while **2** and **3** display a diminished network of interactions with IIA and IIIA sites (Figure 7b,c). IIA residues that participate in HBs with the ligands are located mainly in regions around: Glu188, Lys199, His242, Arg257, Glu292, Glu294, and Lys436.

Similarly, ligand–HSA interactions in the IIIA binding site are governed mostly by the area about Arg410 (including Lys414), Glu382–Asn391, and Glu492. We note that particular HB-participating residues identified here have also been implicated in IIA (Lys199, Arg257, His242) or IIIA (Arg410) binding to HSA.[23] As previously mentioned, **1** is involved in more frequent HBs with multiple HSA residues compared with **2** and **3**; obviously, this is due to structural differences among the groups being attached to the fullerene core of **1**–**3**; namely, **1** possesses larger groups with more HB donor/acceptor sites compared with **2** and **3** (Figure 1b). Nevertheless, all compounds are significantly rigid in each HSA cavity through stabilizing HBs.

To estimate the energy of HBs in a quantitative way, the strength of two interactions in the **2**–HSA complex (IIA-bound form) has been calculated with the AIM method (MP2/6-31G*). The results are shown in the Supporting Information (Figure S9), with the E(HB) values for HB1 and HB2 to be −12.2 and −11.3 kcal/mol, respectively.

III.3. Binding Energies in Fullerene–HSA Complexes. Enthalpy (ΔH), entropy ($-T\Delta S$), and total binding free energy (ΔG_{bind}) contributions have been calculated by using the MM–PBSA approach on the HSA complexes with the fullerene analogs in binding sites IIA and IIIA. The energetic analysis is provided in Table 2 and Table S3. Table 2 summarizes the total binding free energy values for HSA complexes **1**–**3** and C_{60} and provides the enthalpy and entropy contributions on different-length trajectories. Table S3 includes further enthalpy decomposition into individual contributions (e.g., electrostatics, van der Waals, etc.) for complexes **1**–**3**. Moreover, per-residue

DOI: 10.1021/acs.jpcb.5b05998
J. Phys. Chem. B XXXX, XXX, XXX–XXX

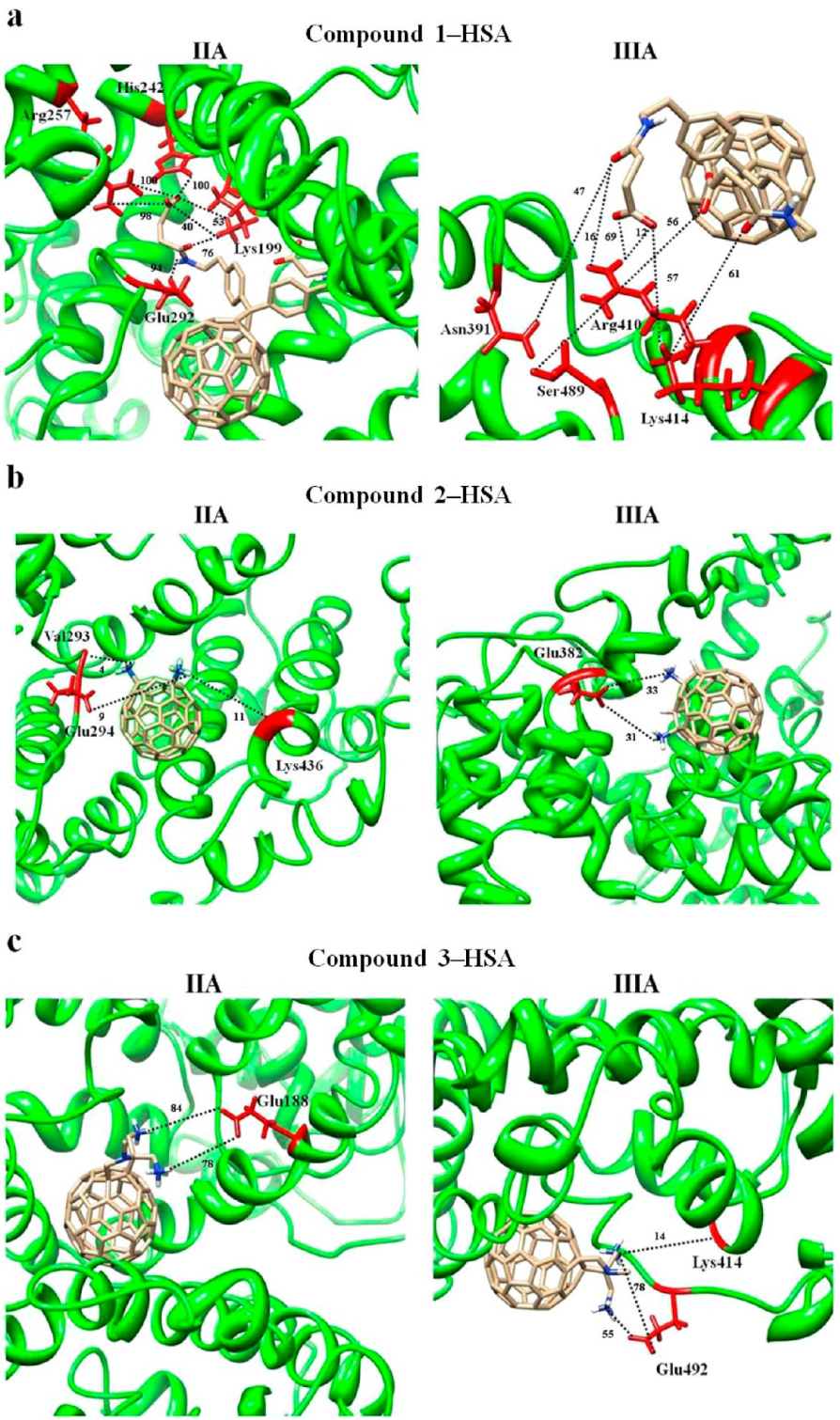

Figure 7. Principal hydrogen bonds (dotted lines) between compounds **1** (a), **2** (b), and **3** (c) and the binding cavities (IIA and IIIA) of HSA. Residues that participate in interactions with the compounds are shown in red. The percentage of time that an HB exists is also denoted.

contributions to the total enthalpy of each system were calculated for HSA complexes with **1**, **2**, and **3**, and residues with major contributions are displayed in Figure 8. Distances (as calculated from the MD trajectories) between fullerenes and the side chains of contributing residues range from 3 to 10 Å. Therefore, the stabilizing residue contributions are anticipated within a radius of 10 Å from the fullerene analog, while the approximate radius of HSA is 40 Å.

It was suggested that significant binding occurs upon fullerene entrapment in each site (IIA or IIIA). **1**–HSA complex formation appears particularly favorable, probably due to the long and negatively charged groups on **1**, which enhance interactions with the binding sites (Table 2). The results of Table 2 show the tendency for more efficient IIA binding compared with IIIA binding because large MM–PBSA energy

DOI: 10.1021/acs.jpcb.5b05998
J. Phys. Chem. B XXXX, XXX, XXX–XXX

Table 2. MM−PBSA Binding Free Energy (ΔG_{bind}) Calculations for HSA Complexes with 1−3 and C_{60} in IIA and IIIA Binding Sites (units are in kcal/mol)[a]

	1		2			3		C_{60}	
compound bind. site	IIA	IIIA	IIA	IIIA	Heme	IIA	IIIA	IIA	IIIA
time (ns)					ΔH				
100[b]	−94.6	−46.0	−40.3	−25.2	−59.0	−50.9	−54.5	−4.9	+5.3
500[c]	−97.4	−55.1				−53.5	−54.4		
550[c]			−39.3	−24.9					
$-T\Delta S$	36.6	24.7	18.1	15.6		25.8	20.9		
ΔG_{bind}[d]	**−60.8**	**−30.4**	**−21.1**	**−9.3**		**−27.8**	**−33.5**		

[a]All numbers correspond to enthalpy (ΔH) values for different simulation times, except the last two lines, where entropy ($-T\Delta S$) and total binding energy (ΔG_{bind}) values are provided. [b]Enthalpy calculations were performed on the last 20 ns of each 100 ns simulation. [c]Enthalpy calculations were performed on the last 250 ns of the 500 or 550 ns trajectory. [d]Enthalpy calculations were performed on ΔG calculations and were based on ΔH values of the longest trajectory for each complex.

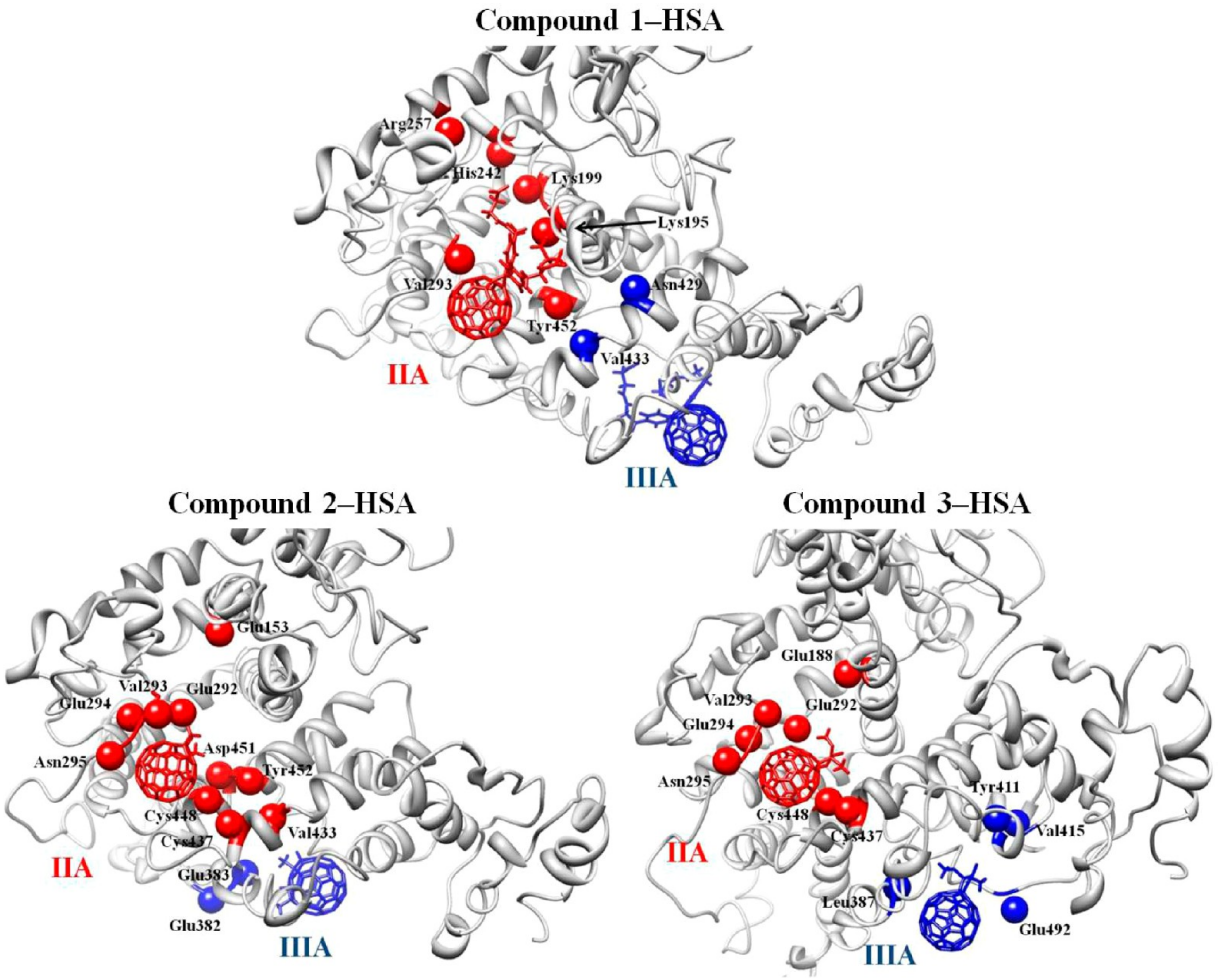

Figure 8. Fullerene derivatives **1**−**3** into the binding cavities IIA and IIIA of HSA. Residues that contribute most favorably to the total enthalpy are shown in red (IIA) and blue (IIIA) spheres.

differences between IIA and IIIA bound HSA complexes were observed (except in **3**−HSA).

Ligand binding in all complexes is driven mostly by van der Waals interactions, followed by the nonpolar contribution to solvation, while the total electrostatics ($\Delta E_{elec}+\Delta G_{PB}$) usually has a negative effect on HSA binding (Table S3). The favorable van der Waals and nonpolar contributions to fullerene−HSA binding are part of a common pattern that has been also observed by our group in various protein systems, including HIV-1 PR,[88−90] renin,[91] κ-opioid receptor,[78] and LOX-1.[79] It is noted that the Coulomb electrostatics term (ΔE_{elec}) is relatively high in all complexes; this is in accordance with previous crystal studies of HSA−myristate in complex with the enantiomers of warfarin in IIA, where it was shown that strong electrostatic interactions were developed between the drug and polar amino acids of HSA.[85,92]

Despite the indications of effective C_{60} binding to HSA (conformational stability as shown in Section III.1), the fullerene core appears to disfavor complex formation (Table

DOI: 10.1021/acs.jpcb.5b05998
J. Phys. Chem. B XXXX, XXX, XXX−XXX

2), thus implying that appropriate groups must be attached to the core to achieve strong binding.

Energy decomposition in a per-residue basis provides useful information on individual contributions to binding. It was shown that for **2**−HSA and **3**−HSA complexes there is a greater number of residues with favorable contributions in IIA than in IIIA (Figure 8). Despite the fact that **2** and **3** stabilize their structures in IIA through different HBs (Figure 7), they share common residues, which contribute favorably to binding. Therefore, two regions within IIA may be distinguished regarding their enthalpy component in each complex (**2** and **3**), namely, Glu292-Val293-Glu294-Asn295 and Cys437/448 were implicated in stabilizing each compound in IIA via major contributions to the binding energy; early crystal studies on the structure of HSA also verify the importance of Glu292 in IIA binding.[23] On the contrary, IIIA binding involves residues, which belong to regions Glu382−Leu387 and around Tyr411−Val415. The IIIA site is located at the outer part of the protein, thus allowing for greater flexibility of the ligand inside the cavity compared with the more engulfed IIA site. Consequently, on the basis of the orientation of the group attached to the fullerene core, the contributing residues may vary significantly. On the basis of this, the groups on **3** acquired a different orientation than that of **2** to include additional contributions from Leu387, Tyr411, Val415, and Glu492 (Figure 8). Additionally, residues Leu387 and Tyr411 were previously implicated in maximizing ligand−IIIA site interactions.[23] Major contributions from HSA residues in **1** binding are also shown in Figure 8.

III.4. Role of the Heme Binding Site. We have performed a 200 ns long MD simulation for **2** bound to the heme site of HSA to account for the behavior of the protein when the heme has been replaced by a fullerene analog. While individual domains and binding sites undergo relatively minor conformational changes, the overall structure of the protein displays a noticeable change during the last 50 ns of the simulation (Figure S10). The average RMSD values for the HSA domains and binding sites when **2** is bound to the heme site are shown in Table 1. Similarly to the other compounds, heme-site binding of **2** decreases the total RMSD of the apo HSA. Moreover, while domain 1 undergoes more substantial conformational changes in the heme-bound form than in the apo form, domain 2 remains practically unaffected by the presence of **2** in the heme site (Table 1). Domain 3, however, stabilized its structure compared with the apo form (4.0 vs 5.8 Å average RMSD for heme-bound and apo HSA, respectively), thus implicating heme-site binding in allosteric modulation of domain 3 (and of IIIA site).

Despite the apparent variability of the heme site, **2** did not show major displacement or other translational/rotational changes during the run. Its presence, however, may have resulted in an increase in the heme site mobility compared with the other forms of HSA. The stability of **2** in the heme site has (at least) partially originated from its HBs with Glu141/167 and Arg186, as obtained from the HB analysis. Table 2 also suggests that binding of **2** to the heme site is favored energetically, similarly to the other binding sites (ΔH_{bind} = −59.0 kcal/mol).

III.5. FMO Analysis of 2−HSA Complexes in Vacuum and Aqueous Environments. *Decomposition Analysis in Water.* To account for a more rigorous description of the fullerene−HSA interactions, FMO calculations in aqueous solution for **2**, bound either to IIA or IIIA, have been performed. The analysis is focused on amino acids based on their proximity to fullerene, their importance in binding (formation of HBs as obtained from the MD analysis), and their positioning at the binding site; for comparison, some random residues that are found in long distance from binding sites (i.e., Tyr353, Met548) were also included. When **2** is bound to IIA, significant electrostatic (including polarization) interactions were observed, mainly involving residues Glu292 and Asp451 (Table S4). These residues belong to the IIA binding cavity and consequently they are in close proximity to the fullerene. Interestingly, the MM−PBSA analysis also showed that the above residues contribute favorably to **2**−IIA complex formation because they are involved in significant interactions with the analog (Figure 8). Surprisingly, noticeable electrostatics were also observed between **2** and other HSA residues (which belong to IIIA or heme site or at random distances away from IIA), such as Glu321, Glu383, Glu492, and Glu141 (Table S4). Favorable electrostatic interactions were predicted for the above residues, although the distances between the fullerene and each residue range from ∼6 to ∼17 Å. It is, however, noted that because the charge of the fullerene is +2, enhanced electrostatics with negatively charged residues, such as Glu and Asp, may be anticipated. It is therefore expected that HSA amino acids with positive charge would disfavor interactions with **2**. Thus, residues Lys195/199/413/414/436 and Arg114/186/218/257/410 participate in most unfavorable electrostatics with **2**.

Similar observations associate Glu383 and Glu492 with the fullerene, when the latter is bound to IIIA. In agreement with the MM−PBSA energy decomposition analysis, the FMO calculation showed Glu383 to contribute significantly to the binding energy of the IIIA complex (Figure 8). Table S5 shows that **2** interacts mainly with these two residues in IIIA; however, similarly to the IIA-bound structure, negatively charged Asp and Glu that are far away from IIIA also display enhanced interactions with **2**, while positively charged Lys and Arg developed unfavorable electrostatics with the fullerene.

For residues that are closer than 2.0 Å to **2**, further energy decomposition to include charge, dispersion, and exchange energy terms was carried out. It was generally observed that the exchange energy (E_{ex}) disfavors either IIA or IIIA complex formation, while the sum E_{ct+mix} favors **2**−HSA interactions (Tables S4 and S5). Importantly, our calculations predicted that although the dispersion energy (E_{disp}) term is small, it is the second most important driving force (after electrostatics) for the stabilization of **2**−HSA complex.

Decomposition Analysis in Vacuo. The above calculations have been also performed for **2** into IIA in the absence of water molecules. Tables S4 and S5 indicate that the water environment has a rather minor effect on the binding properties of the system.

The FMO analysis provided additional energy terms (ΔE_{ex}, ΔE_{ct+mix}, ΔE_{disp}, eq S1) and rationalized the MM−PBSA results for **2**−HSA because it verified (in a more rigorous fashion) the principal interactions in IIA (involving Glu292 and Asp451) and IIIA (involving Glu383) sites. Moreover, the results of Tables S4 and S5 provided further support to the indication of more efficient IIA than IIIA binding (MM−PBSA results, Section III.4).

III.6. Energy Decomposition Analysis. To broaden our investigation, we have selected the truncated fullerene−HSA systems A and B (Figure S11), which involve the interaction of fullerenes **2** and **3**, respectively, with crucial protein residues in

DOI: 10.1021/acs.jpcb.5b05998
J. Phys. Chem. B XXXX, XXX, XXX−XXX

the IIA binding cavity because it was found that in most cases binding to IIA is stronger than in IIIA (Table 2). In combination with the FMO analysis, the EDA method provides a detailed understanding of the interaction of fullerene−HSA fragments using QM methods (DFT, MP2). Moreover, additional contributions, E_{rep} and E_{pol}, are included in the analysis of the interaction between fullerenes and HSA. Systems A and B have total charges Q = 0.0 and 3.0e, respectively, while the charge of each fullerene is 2.0. Geometries correspond to the average structures, as obtained from the MD trajectories of the fullerenes with HSA. These computations allow a detailed understanding of some interacting fragments of the fullerene−HSA complex. In Table 3, the results for the resolution of the

Table 3. Energy Decomposition Analysis of the Interacting Systems (Figure S11) Based on the EDA Scheme and Computed by Employing a Series of Methods[a]

system term	A	B
E_{el}	−210.71[b]	46.57[c]
	−224.24[c]	47.41[f]
		47.37[g]
E_{ex}	−48.98[b]	−13.06[c]
	−47.83[c]	−4.98[f]
		−6.94[g]
E_{rep}	88.69[b]	24.82[c]
	86.69[c]	20.31[f]
		22.07[g]
E_{pol}	−46.39[b]	−12.29[c]
	−46.53[c]	−13.45[f]
		−12.80[g]
E_{disp}	−3.99[d]	−3.56[f]
	−10.88[e]	−5.59[g]
E_{tot} (= ΔE)	−217.19[b]	46.05[c]
	−231.91[c]	45.73[f]
	−235.90[d]	44.12[g]
	−228.07[e]	

[a]All values are in kilocalories per mole. [b]Method: HF/6-31G*. [c]Method: HF/3-21G*. [d]Method: MP2/3-21G*. [e]Method: MP2/6-31G*. [f]Method: B3LYP/3-21G*. [g]Method: M06-2X/3-21G*.

interaction energy E_{tot} (= ΔE) are reported. A series of methods (HF, MP2, DFT) and basis sets (3-21G*, 6-31G*) have been used. Systems A and B have large E_{el} contribution, which is the dominant term in E_{tot}. For both A and B, the sign of E_{tot}, which indicates whether binding is favorable, depends on the sign of the E_{el} term; this is negative for A and positive for B. For A, the contribution of E_{ex} + E_{rep} + E_{pol} is −7.7 kcal/mol (HF/3-21G*), being significantly smaller than E_{el}. For B, this sum is −0.53 kcal/mol. For A and B, the dispersion correction (E_{disp}) is small. It was shown that the variation of basis sets (3-21G*, 6-31G*) does not affect remarkably the various energy terms. This is important because the use of high-level theories (e.g., MP2, CCSD) and large basis sets increases significantly the computational cost.

In summary, the EDA electrostatic term (E_{el}) dominates the total energy contribution in fullerene−HSA systems A and B (Figure S11 and Table 3). The E_{el} values (EDA) show the same pattern with the MM−PBSA electrostatics (ΔE_{elec}, Table S8). Therefore, the above analyses (Sections III.5 and III.6) based on rigorous QM approaches confirm the MM−PBSA method regarding charge interactions between fullerene and HSA, thus indicating the suitability of MM−PBSA to describe reliably the individual electrostatics in the HSA complexes.

IV. CONCLUSIONS

A comprehensive computational study has been attempted to elucidate the binding mechanism in the two main binding sites (IIA and IIIA) of HSA in complexes with fullerene analogs. A broad range of computational techniques (MD, MM−PBSA, fragment molecular orbital, energy decomposition analysis, and atoms-in-molecules) has been applied to explore the modes of binding and the principal interactions that govern the fullerene−HSA association. Several of our findings have been confirmed by experimental or other theoretical studies.

The main elements of fullerene binding to HSA are:

(1) The apo form of HSA is more variable and less compact than its fullerene-bound forms. IIA and IIIA binding sites are stabilized upon binding, while the IIIA complexes are more mobile than the IIA complexes. The overall HSA shape and secondary structure characteristics were found to remain unchanged upon binding, with subtle variations observed in the α-helix and β-turn contents.

(2) Fullerene binding to IIA is potentially associated with allosteric modulation. Binding of derivatives **1**−**3** to IIA results in a profound inward motion of the IIIB subdomain (45.5−68.9° rotation) and secondary structure changes in IIIA; in the case of **2** and **3** this is accompanied by movement of the IB (heme site) and IA subdomains, respectively. This is in agreement with experimental data, which suggest that IIA site-specific binding of several ligands results in allosteric modulation of the heme site.[93−95]

(3) All fullerene analogs were practically stable in the binding sites of HSA.

(4) Compounds were stabilized in either cavity of HSA through multiple and diverse HB interactions. Residues that involve HBs with the ligands include: Glu188/292, Lys199, His242, Arg257 (IIA site) and Arg410, Glu382−Asn391, Lys414, Glu492 (IIIA site).

(5) All fullerenes display significant binding affinities for HSA, with MM−PBSA free-energy values ranging from −10 to −60 kcal/mol; IIA binding is more efficient that IIIA binding. Residues Glu292−Asn295 and Cys437/448 contribute favorably to IIA binding, while Glu382/383/492, Leu387, Tyr411, and Val415 were associated with binding to IIIA site.

(6) Binding is driven by van der Waals, nonpolar, charge transfer, and dispersion energy contributions; the exchange energy and the total electrostatics (Coulomb part and the contribution to the solvation free energy) disfavor fullerene−HSA complex formation.

(7) Long and negatively charged groups attached to the fullerene core may be necessary to enhance ligand−HSA interactions. Negatively charged fullerene adducts are efficiently bound to HSA, in agreement with previous studies, which highlighted the ability of hydrophobic HSA domains to host anionic and neutral species;[96,97] only a limited number of cationic compounds have been reported to exempt this rule.[98] Our computations showed that it is possible to bring positively charged species in IIA cavity, although binding was found to be weaker than with their negatively charged counterparts.

The above findings have significant biological implications: The remarkable binding of certain fullerenes to HSA may facilitate their transfer (by HSA) and availability at critical organs (e.g., brain), thus enhancing their usefulness in therapies (e.g., photodynamic treatment).

DOI: 10.1021/acs.jpcb.5b05998
J. Phys. Chem. B XXXX, XXX, XXX−XXX

■ ASSOCIATED CONTENT

Supporting Information

The Supporting Information is available free of charge on the ACS Publications website at DOI: 10.1021/acs.jpcb.5b05998.

Details of clustering, secondary structure, dynamic domain, and FMO analyses. Additional results on: apo HSA, **2**−HSA (bound to the heme site), C_{60}−HSA; AIM calculations for **2**; MM−PBSA, EDA analyses for selected systems. (PDF)

Movie file illustrating dynamic domain movements for **2**. (AVI)

■ AUTHOR INFORMATION

Corresponding Authors

*G.L.: E-mail: georgios.leonis@gmail.com. Tel: 0030-210-727-3894.

*M.G.P.: E-mail: mpapad@eie.gr. Tel: 0030-210-727-3892.

Notes

The authors declare no competing financial interest.

■ ACKNOWLEDGMENTS

This work was supported by the European Commission for FP7-PEOPLE-2011-IRSES project "NanoBRIDGES" (grant agreement no. PIRSES-GA-2011-295128) and project "Nano-PUZZLES" (grant agreement no. NMPSL-2012-309837). Additional support was offered by LinkSCEEM-2 project, funded by the European Commission under the 7th Framework Programme through Capacities Research Infrastructure, INFRA-2010-1.2.3 Virtual Research Communities, Combination of Collaborative Project and Coordination and Support Actions (CP-CSA) under grant agreement no. RI-261600. We also thank PRACE for awarding us access to resource Curie (Hybrid nodes) at Bruyères-Le-Châtel, France and the supercomputer MareNostrum at Barcelona Supercomputing Center−Centro Nacional de Supercomputación (The Spanish National Supercomputing Center) for facilitating parts of the MD simulations.

■ REFERENCES

(1) Mu, Q.; Jiang, G.; Chen, L.; Zhou, H.; Fourches, D.; Tropsha, A.; Yan, B. Chemical basis of interactions between engineered nanoparticles and biological systems. *Chem. Rev.* **2014**, *114*, 7740−7781.

(2) Karmali, P. P.; Simberg, D. Interactions of nanoparticles with plasma proteins: implication on clearance and toxicity of drug delivery systems. *Expert Opin. Drug Delivery* **2011**, *8*, 343−357.

(3) Lewinski, N.; Colvin, V.; Drezek, R. Cytotoxicity of nanoparticles. *Small* **2008**, *4*, 26−49.

(4) Cedervall, T.; Lynch, I.; Lindman, S.; Berggard, T.; Thulin, E.; Nilsson, H.; Dawson, K. A.; Linse, S. Understanding the nanoparticle-protein corona using methods to quantify exchange rates and affinities of proteins for nanoparticles. *Proc. Natl. Acad. Sci. U. S. A.* **2007**, *104*, 2050−2055.

(5) Sharifi, S.; Behzadi, S.; Laurent, S.; Forrest, M. L.; Stroeve, P.; Mahmoudi, M. Toxicity of nanomaterials. *Chem. Soc. Rev.* **2012**, *41*, 2323−2343.

(6) Nienhaus, G. U.; Maffre, P.; Nienhaus, K. Studying the protein corona on nanoparticles by FCS. *Methods Enzymol.* **2013**, *519*, 115−137.

(7) Bamrungsap, S.; Zhao, Z. L.; Chen, T.; Wang, L.; Li, C. M.; Fu, T.; Tan, W. H. Nanotechnology in therapeutics: a focus on nanoparticles as a drug delivery system. *Nanomedicine* **2012**, *7*, 1253−1271.

(8) Calvaresi, M.; Zerbetto, F. Fullerene sorting proteins. *Nanoscale* **2011**, *3*, 2873−2881.

(9) Calvaresi, M.; Zerbetto, F. Baiting proteins with C-60. *ACS Nano* **2010**, *4*, 2283−2299.

(10) Innocenti, A.; Durdagi, S.; Doostdar, N.; Strom, T. A.; Barron, A. R.; Supuran, C. T. Nanoscale enzyme inhibitors: fullerenes inhibit carbonic anhydrase by occluding the active site entrance. *Bioorg. Med. Chem.* **2010**, *18*, 2822−2828.

(11) Durdagi, S.; Supuran, C. T.; Strom, T. A.; Doostdar, N.; Kumar, M. K.; Barron, A. R.; Mavromoustakos, T.; Papadopoulos, M. G. In silico drug screening approach for the design of magic bullets: a successful example with anti-HIV fullerene derivatized amino acids. *J. Chem. Inf. Model.* **2009**, *49*, 1139−1143.

(12) Thakral, S.; Thakral, N. K. Potential Medical Applications of Fullerenes: An Overview. In *Bio-Nanotechnology*; Wiley-Blackwell: Chichester, U.K., 2013; pp 424−441.

(13) Cui, Q.; Yang, X.; Ebrahimi, A.; Li, J. Fullerene−biomolecule conjugates and their biomedicinal applications. *Int. J. Nanomed.* **2013**, *9*, 77−92.

(14) Sapsford, K. E.; Algar, W. R.; Berti, L.; Gemmill, K. B.; Casey, B. J.; Oh, E.; Stewart, M. H.; Medintz, I. L. Functionalizing nanoparticles with biological molecules: Developing chemistries that facilitate nanotechnology. *Chem. Rev.* **2013**, *113*, 1904−2074.

(15) Bakry, R.; Vallant, R. M.; Najam-Ul-Haq, M.; Rainer, M.; Szabo, Z.; Huck, C. W.; Bonn, G. K. Medicinal applications of fullerenes. *Int. J. Nanomed.* **2007**, *2*, 639−649.

(16) Bosi, S.; Da Ros, T.; Spalluto, G.; Balzarini, J.; Prato, M. Synthesis and anti-HIV properties of new water-soluble bis-functionalized[60]fullerene derivatives. *Bioorg. Med. Chem. Lett.* **2003**, *13*, 4437−4440.

(17) Huy, P. D. Q.; Li, M. S. Binding of fullerenes to amyloid beta fibrils: size matters. *Phys. Chem. Chem. Phys.* **2014**, *16*, 20030−20040.

(18) Nicholson, J. P.; Wolmarans, M. R.; Park, G. R. The role of albumin in critical illness. *Brit J. Anaesth* **2000**, *85*, 599−610.

(19) Kratz, F. A clinical update of using albumin as a drug vehicle - A commentary. *J. Controlled Release* **2014**, *190*, 331−336.

(20) Yang, F.; Zhang, Y.; Liang, H. Interactive association of drugs binding to human serum albumin. *Int. J. Mol. Sci.* **2014**, *15*, 3580−3595.

(21) Fasano, M.; Curry, S.; Terreno, E.; Galliano, M.; Fanali, G.; Narciso, P.; Notari, S.; Ascenzi, P. The extraordinary ligand binding properties of human serum albumin. *IUBMB Life* **2005**, *57*, 787−796.

(22) Zhang, X.-f.; Shu, C.-y.; Xie, L.; Wang, C.-r.; Zhang, Y.-z.; Xiang, J.-f.; Li, L.; Tang, Y.-l. Protein conformation changes induced by a novel organophosphate-containing water-soluble derivative of a C60 fullerene nanoparticle. *J. Phys. Chem. C* **2007**, *111*, 14327−14333.

(23) He, X. M.; Carter, D. C. Atomic-structure and chemistry of human serum-albumin. *Nature* **1992**, *358*, 209−215.

(24) Artali, R.; Bombieri, G.; Calabi, L.; Del Pra, A. A molecular dynamics study of human serum albumin binding sites. *Farmaco* **2005**, *60*, 485−495.

(25) Qu, X.; Komatsu, T.; Sato, T.; Glatter, O.; Horinouchi, H.; Kobayashi, K.; Tsuchida, E. Structure, photophysical property, and cytotoxicity of human serum albumin complexed with tris-(dicarboxymethylene)[60]fullerene. *Bioconjugate Chem.* **2008**, *19*, 1556−1560.

(26) Zhang, M. F.; Xu, Z. Q.; Ge, Y. S.; Jiang, F. L.; Liu, Y. Binding of fullerol to human serum albumin: spectroscopic and electrochemical approach. *J. Photochem. Photobiol., B* **2012**, *108*, 34−43.

(27) Zhen, M.; Zheng, J.; Ye, L.; Li, S.; Jin, C.; Li, K.; Qiu, D.; Han, H.; Shu, C.; Yang, Y.; et al. Maximizing the relaxivity of Gd-complex by synergistic effect of HSA and carboxylfullerene. *ACS Appl. Mater. Interfaces* **2012**, *4*, 3724−3729.

(28) Abdulmalik, A.; Hibah, A.; Zainy, B. M.; Makoto, A.; Daisuke, I.; Masaki, O.; Kaneto, U.; Fumitoshi, H. Preparation of soluble stable C60/human serum albumin nanoparticles via cyclodextrin complexation and their reactive oxygen production characteristics. *Life Sci.* **2013**, *93*, 277−282.

(29) Song, M.; Liu, S.; Yin, J.; Wang, H. Interaction of human serum album and C(60) aggregates in solution. *Int. J. Mol. Sci.* **2011**, *12*, 4964−4974.

(30) Li, S.; Zhao, X. C.; Mo, Y. M.; Cummings, P. T.; Heller, W. T. Human serum albumin interactions with C-60 fullerene studied by spectroscopy, small-angle neutron scattering, and molecular dynamics simulations. *J. Nanopart. Res.* **2013**, *15*, 1769.
(31) Rozhkov, S. P.; Goryunov, A. S.; Sukhanova, G. A.; Borisova, A. G.; Rozhkova, N. N.; Andrievsky, G. V. Protein interaction with hydrated C60 fullerene in aqueous solutions. *Biochem. Biophys. Res. Commun.* **2003**, *303*, 562−566.
(32) Belgorodsky, B.; Fadeev, L.; Ittah, V.; Benyamini, H.; Zelner, S.; Huppert, D.; Kotlyar, A. B.; Gozin, M. Formation and characterization of stable human serum albumin-tris-malonic acid [C-60]fullerene complex. *Bioconjugate Chem.* **2005**, *16*, 1058−1062.
(33) Benyamini, H.; Shulman-Peleg, A.; Wolfson, H. J.; Belgorodsky, B.; Fadeev, L.; Gozin, M. Interaction of C-60-fullerene and carboxyfullerene with proteins: Docking and binding site alignment. *Bioconjugate Chem.* **2006**, *17*, 378−386.
(34) Sudlow, G.; Birkett, D. J.; Wade, D. N. The characterization of two specific drug binding sites on human serum albumin. *Mol. Pharmacol.* **1975**, *11*, 824−832.
(35) Vallant, R. M.; Szabo, Z.; Trojer, L.; Najam-ul-Haq, M.; Rainer, M.; Huck, C. W.; Bakry, R.; Bonn, G. K. A new analytical material-enhanced laser desorption ionization (MELDI) based approach for the determination of low-mass serum constituents using fullerene derivatives for selective enrichment. *J. Proteome Res.* **2007**, *6*, 44−53.
(36) Kayat, J.; Gajbhiye, V.; Tekade, R. K.; Jain, N. K. Pulmonary toxicity of carbon nanotubes: a systematic report. *Nanomedicine* **2011**, *7*, 40−49.
(37) Bobylev, A. G.; Kornev, A. B.; Bobyleva, L. G.; Shpagina, M. D.; Fadeeva, I. S.; Fadeev, R. S.; Deryabin, D. G.; Balzarini, J.; Troshin, P. A.; Podlubnaya, Z. A. Fullerenolates: metallated polyhydroxylated fullerenes with potent anti-amyloid activity. *Org. Biomol. Chem.* **2011**, *9*, 5714−5719.
(38) Piette, J. Mutagenic and genotoxic properties of singlet oxygen. *J. Photochem. Photobiol., B* **1990**, *4*, 335−339.
(39) Komatsu, T.; Nakagawa, A.; Qu, X. Structural and mutagenic approach to create human serum albumin-based oxygen carrier and photosensitizer. *Drug Metab. Pharmacokinet.* **2009**, *24*, 287−299.
(40) The ground state of $^1C_{60}$ is excited by visible light to $^1C_{60}$* (singlet excited state), and a conversion to $^3C_{60}$* follows; an intersystem crossing is involved. Then $^3C_{60}$* transfers energy to $^3O_2$, and $^1O_2$ is generated (type II energy transfer) [*JACS*, 120, 12363 (1998); *JACS*, 121, 464 (1999)]. Photodynamic therapy applications involve three components: a photosensitizer (PS), a light source, and oxygen (tissue). The above components produce reactive species (e.g., $^1O_2$) in a localized area, which lead to cell destruction. Several pathways may be involved for this destruction, the most important of which is DNA strand cleavage [*JACS*, 125, 12803 (2003)]. A photosensitizer is a strongly absorbing molecule, which is excited into a singlet state. Fullerenes are excellent PSs. They absorb strongly in the UV and moderately in the visible regions of the spectrum [*Biorg. Med. Chem.*, 4, 767 (1996)].
(41) Graves, A. P.; Shivakumar, D. M.; Boyce, S. E.; Jacobson, M. P.; Case, D. A.; Shoichet, B. K. Rescoring docking hit lists for model cavity sites: predictions and experimental testing. *J. Mol. Biol.* **2008**, *377*, 914−934.
(42) Wang, J.; Wang, W.; Kollman, P. A.; Case, D. A. Automatic atom type and bond type perception in molecular mechanical calculations. *J. Mol. Graphics Modell.* **2006**, *25*, 247−260.
(43) Case, D. A.; Darden, T. A.; Cheatham, T. E.; Simmerling, C. L.; Wang, J.; Duke, R. E.; Luo, R.; Walker, R. C.; Zhang, W.; Merz, K. M. *AMBER 12*; University of California: San Francisco, 2012.
(44) Salomon-Ferrer, R.; Case, D. A.; Walker, R. C. An overview of the Amber biomolecular simulation package. *Wiley Interdiscip. Rev.: Comput. Mol. Sci.* **2013**, *3*, 198−210.
(45) Wang, J.; Wolf, R. M.; Caldwell, J. W.; Kollman, P. A.; Case, D. A. Development and testing of a general amber force field. *J. Comput. Chem.* **2004**, *25*, 1157−1174.
(46) Hornak, V.; Abel, R.; Okur, A.; Strockbine, B.; Roitberg, A.; Simmerling, C. Comparison of multiple Amber force fields and development of improved protein backbone parameters. *Proteins: Struct., Funct., Genet.* **2006**, *65*, 712−725.
(47) Jorgensen, W. L.; Chandrasekhar, J.; Madura, J. D.; Impey, R. W.; Klein, M. L. Comparison of simple potential functions for simulationg liquid water. *J. Chem. Phys.* **1983**, *79*, 926−935.
(48) Izaguirre, J. A.; Catarello, D. P.; Wozniak, J. M.; Skeel, R. D. Langevin stabilization of molecular dynamics. *J. Chem. Phys.* **2001**, *114*, 2090−2098.
(49) Salomon-Ferrer, R.; Götz, A. W.; Poole, D.; Le Grand, S.; Walker, R. C. Routine microsecond molecular dynamics simulations with AMBER on GPUs. 2. Explicit solvent particle mesh Ewald. *J. Chem. Theory Comput.* **2013**, *9*, 3878−3888.
(50) Götz, A. W.; Williamson, M. J.; Xu, D.; Poole, D.; Le Grand, S.; Walker, R. C. Routine microsecond molecular dynamics simulations with AMBER on GPUs. 1. Generalized Born. *J. Chem. Theory Comput.* **2012**, *8*, 1542−1555.
(51) Le Grand, S.; Götz, A. W.; Walker, R. C. SPFP: Speed without compromise—A mixed precision model for GPU accelerated molecular dynamics simulations. *Comput. Phys. Commun.* **2013**, *184*, 374−380.
(52) Ryckaert, J. P.; Ciccotti, G.; Berendsen, H. J. C. Numerical integration of the Cartesian equations of motion of a system with constraints: Molecular dynamics of n-alkanes. *J. Comput. Phys.* **1977**, *23*, 327−341.
(53) Daura, X.; Gademann, K.; Jaun, B.; Seebach, D.; van Gunsteren, W. F.; Mark, A. E. Peptide folding: When simulation meets experiment. *Angew. Chem., Int. Ed.* **1999**, *38*, 236−240.
(54) Hess, B.; Kutzner, C.; van der Spoel, D.; Lindahl, E. GROMACS 4: Algorithms for highly efficient, load-balanced, and scalable molecular simulation. *J. Chem. Theory Comput.* **2008**, *4*, 435−447.
(55) Hayward, S.; Berendsen, H. J. Systematic analysis of domain motions in proteins from conformational change: new results on citrate synthase and T4 lysozyme. *Proteins: Struct., Funct., Genet.* **1998**, *30*, 144−154.
(56) Kollman, P. A.; Massova, I.; Reyes, C.; Kuhn, B.; Huo, S.; Chong, L.; Lee, M.; Lee, T.; Duan, Y.; Wang, W.; et al. Calculating structures and free energies of complex molecules: combining molecular mechanics and continuum models. *Acc. Chem. Res.* **2000**, *33*, 889−897.
(57) Gohlke, H.; Kiel, C.; Case, D. A. Insights into protein-protein binding by binding free energy calculation and free energy decomposition for the Ras-Raf and Ras-RalGDS complexes. *J. Mol. Biol.* **2003**, *330*, 891−913.
(58) Leonis, G.; Steinbrecher, T.; Papadopoulos, M. G. A contribution to the drug resistance mechanism of darunavir, amprenavir, indinavir, and saquinavir complexes with HIV-1 protease due to flap mutation I50V: a systematic MM-PBSA and thermodynamic integration study. *J. Chem. Inf. Model.* **2013**, *53*, 2141−2153.
(59) Hou, T.; Wang, J.; Li, Y.; Wang, W. Assessing the performance of the MM/PBSA and MM/GBSA methods. 1. The accuracy of binding free energy calculations based on molecular dynamics simulations. *J. Chem. Inf. Model.* **2011**, *51*, 69−82.
(60) Cao, R.; Huang, N.; Wang, Y. Evaluation and application of MD-PB/SA in structure-based hierarchical virtual screening. *J. Chem. Inf. Model.* **2014**, *54*, 1987−1996.
(61) Uciechowska, U.; Schemies, J.; Neugebauer, R. C.; Huda, E. M.; Schmitt, M. L.; Meier, R.; Verdin, E.; Jung, M.; Sippl, W. Thiobarbiturates as sirtuin inhibitors: virtual screening, free-energy calculations, and biological testing. *ChemMedChem* **2008**, *3*, 1965−1976.
(62) Kumar, A.; Ito, A.; Hirohama, M.; Yoshida, M.; Zhang, K. Y. Identification of sumoylation activating enzyme 1 inhibitors by structure-based virtual screening. *J. Chem. Inf. Model.* **2013**, *53*, 809−820.
(63) Chen, Y.; Fang, L.; Peng, S.; Liao, H.; Lehmann, J.; Zhang, Y. Discovery of a novel acetylcholinesterase inhibitor by structure-based virtual screening techniques. *Bioorg. Med. Chem. Lett.* **2012**, *22*, 3181−3187.

DOI: 10.1021/acs.jpcb.5b05998
J. Phys. Chem. B XXXX, XXX, XXX−XXX

(64) Venken, T.; Krnavek, D.; Munch, J.; Kirchhoff, F.; Henklein, P.; De Maeyer, M.; Voet, A. An optimized MM/PBSA virtual screening approach applied to an HIV-1 gp41 fusion peptide inhibitor. *Proteins: Struct., Funct., Genet.* **2011**, *79*, 3221−3235.
(65) Ferrari, A. M.; Degliesposti, G.; Sgobba, M.; Rastelli, G. Validation of an automated procedure for the prediction of relative free energies of binding on a set of aldose reductase inhibitors. *Bioorg. Med. Chem.* **2007**, *15*, 7865−7877.
(66) Tzoupis, H.; Leonis, G.; Avramopoulos, A.; Reis, H.; Czyżnikowska, Z.; Zerva, S.; Vergadou, N.; Peristeras, L. D.; Papavasileiou, K. D.; et al. Alexis, et al., Elucidation of the binding mechanism of renin using a wide array of computational techniques and biological assays. *J. Mol. Graphics Modell.* **2015**, *62*, 138−149.
(67) Kitaura, K.; Morokuma, K. New energy decomposition scheme for molecular-interactions within Hartree-Fock approximation. *Int. J. Quantum Chem.* **1976**, *10*, 325−340.
(68) Morokuma, K. Molecular Orbital Studies of Hydrogen Bonds. III. C═O···H−O hydrogen bond in H2CO···H2O and H2CO···2H2O. *J. Chem. Phys.* **1971**, *55*, 1236−1244.
(69) Fedorov, D.; Kitaura, K. *The Fragment Molecular Orbital Method: Practical Applications to Large Molecular Systems*; CRC Press: Boca Raton, FL, 2009.
(70) Fedorov, D. G.; Kitaura, K. Pair interaction energy decomposition analysis. *J. Comput. Chem.* **2007**, *28*, 222−237.
(71) Schmidt, M. W.; Baldridge, K. K.; Boatz, J. A.; Elbert, S. T.; Gordon, M. S.; Jensen, J. H.; Koseki, S.; Matsunaga, N.; Nguyen, K. A.; Su, S. J.; et al. General atomic and molecular electronic-structure system. *J. Comput. Chem.* **1993**, *14*, 1347−1363.
(72) Su, P.; Li, H. Energy decomposition analysis of covalent bonds and intermolecular interactions. *J. Chem. Phys.* **2009**, *131*, 014102.
(73) Boys, S. F.; Bernardi, F. Calculation of small molecular interactions by differences of separate total energies - Some procedures with reduced errors. *Mol. Phys.* **1970**, *19*, 553−566.
(74) Bader, R. F. W. *Atoms in Molecules: A Quantum Theory*; Clarendon: Oxford, U.K., 1990.
(75) Espinosa, E.; Molins, E.; Lecomte, C. Hydrogen bond strengths revealed by topological analyses of experimentally observed electron densities. *Chem. Phys. Lett.* **1998**, *285*, 170−173.
(76) Frisch, M. J.; Trucks, G. W.; Schlegel, H. B.; Scuseria, G. E.; Robb, M. A.; Cheeseman, J. R.; Scalmani, G.; Barone, V.; Mennucci, B.; Petersson, G. A.; et al. *Gaussian 09*, Revision A; Gaussian, Inc.: Wallingford, CT, 2009.
(77) Biegler-Konig, F.; Schonbohm, J. Update of the AIM2000-program for atoms in molecules. *J. Comput. Chem.* **2002**, *23*, 1489−1494.
(78) Leonis, G.; Avramopoulos, A.; Salmas, R. E.; Durdagi, S.; Yurtsever, M.; Papadopoulos, M. G. Elucidation of conformational states, dynamics, and mechanism of binding in human kappa-opioid receptor complexes. *J. Chem. Inf. Model.* **2014**, *54*, 2294−2308.
(79) Vrontaki, E.; Leonis, G.; Avramopoulos, A.; Papadopoulos, M. G.; Simcic, M.; Grdadolnik, S. G.; Afantitis, A.; Melagraki, G.; Hadjikakou, S. K.; Mavromoustakos, T. Stability and binding effects of silver(I) complexes at lipoxygenase-1. *J. Enzyme Inhib. Med. Chem.* **2015**, *30*, 539−549.
(80) Fanali, G.; Rampoldi, V.; Masi, A. d.; Bolli, A.; Lopiano, L.; Ascenzi, P.; Fasano, M. Binding of anti-Parkinson's disease drugs to human serum albumin is allosterically modulated. *IUBMB Life* **2010**, *62*, 371−376.
(81) Guizado, T. R. Analysis of the structure and dynamics of human serum albumin. *J. Mol. Model.* **2014**, *20*, 2450.
(82) Curry, S.; Mandelkow, H.; Brick, P.; Franks, N. Crystal structure of human serum albumin complexed with fatty acid reveals an asymmetric distribution of binding sites. *Nat. Struct. Biol.* **1998**, *5*, 827−835.
(83) Sugio, S.; Kashima, A.; Mochizuki, S.; Noda, M.; Kobayashi, K. Crystal structure of human serum albumin at 2.5 A resolution. *Protein Eng., Des. Sel.* **1999**, *12*, 439−446.
(84) Petitpas, I.; Grune, T.; Bhattacharya, A. A.; Curry, S. Crystal structures of human serum albumin complexed with monounsaturated and polyunsaturated fatty acids. *J. Mol. Biol.* **2001**, *314*, 955−960.
(85) Colmenarejo, G. In silico prediction of drug-binding strengths to human serum albumin. *Med. Res. Rev.* **2003**, *23*, 275−301.
(86) Fujiwara, S.-i.; Amisaki, T. Molecular dynamics study of conformational changes in human serum albumin by binding of fatty acids. *Proteins: Struct., Funct., Genet.* **2006**, *64*, 730−739.
(87) Paris, G.; Ramseyer, C.; Enescu, M. A principal component analysis of the dynamics of subdomains and binding sites in human serum albumin. *Biopolymers* **2014**, *101*, 561−572.
(88) Leonis, G.; Czyznikowska, Z.; Megariotis, G.; Reis, H.; Papadopoulos, M. G. Computational studies of darunavir into HIV-1 protease and DMPC bilayer: necessary conditions for effective binding and the role of the flaps. *J. Chem. Inf. Model.* **2012**, *52*, 1542−58.
(89) Tzoupis, H.; Leonis, G.; Durdagi, S.; Mouchlis, V.; Mavromoustakos, T.; Papadopoulos, M. G. Binding of novel fullerene inhibitors to HIV-1 protease: insight through molecular dynamics and molecular mechanics Poisson-Boltzmann surface area calculations. *J. Comput.-Aided Mol. Des.* **2011**, *25*, 959−976.
(90) Tzoupis, H.; Leonis, G.; Megariotis, G.; Supuran, C. T.; Mavromoustakos, T.; Papadopoulos, M. G. Dual inhibitors for aspartic proteases HIV-1 PR and renin: advancements in AIDS-hypertension-diabetes linkage via molecular dynamics, inhibition assays, and binding free energy calculations. *J. Med. Chem.* **2012**, *55*, 5784−5796.
(91) Politi, A.; Leonis, G.; Tzoupis, H.; Ntountaniotis, D.; Papadopoulos, M. G.; Grdadolnik, S. G.; Mavromoustakos, T. Conformational properties and energetic analysis of aliskiren in solution and receptor site. *Mol. Inf.* **2011**, *30*, 973−985.
(92) Petitpas, I.; Bhattacharya, A. A.; Twine, S.; East, M.; Curry, S. Crystal structure analysis of warfarin binding to human serum albumin: anatomy of drug site I. *J. Biol. Chem.* **2001**, *276*, 22804−22809.
(93) Ascenzi, P.; Bocedi, A.; Notari, S.; Fanali, G.; Fesce, R.; Fasano, M. Allosteric modulation of drug binding to human serum albumin. *Mini-Rev. Med. Chem.* **2006**, *6*, 483−489.
(94) Ascenzi, P.; Fasano, M. Allostery in a monomeric protein: The case of human serum albumin. *Biophys. Chem.* **2010**, *148*, 16−22.
(95) Fanali, G.; Rampoldi, V.; di Masi, A.; Bolli, A.; Lopiano, L.; Ascenzi, P.; Fasano, M. Binding of anti-Parkinson's disease drugs to human serum albumin is allosterically modulated. *IUBMB Life* **2010**, *62*, 371−376.
(96) Peters, T., Jr. 3 - Ligand Binding by Albumin. In *All about Albumin*; Peters, T., Ed.; Academic Press: San Diego, 1995; pp 76−132.
(97) Wanwimolruk, S.; Birkett, D. J.; Brooks, P. M. Structural requirements for drug binding to site II on human serum albumin. *Mol. Pharmacol.* **1983**, *24*, 458−463.
(98) Kragh-Hansen, U. Molecular aspects of ligand binding to serum albumin. *Pharmacol. Rev.* **1981**, *33*, 17−53.

DOI: 10.1021/acs.jpcb.5b05998
J. Phys. Chem. B XXXX, XXX, XXX−XXX